Finite volume solution of a 2-D lid driven cavity flow in unsteady state and at high Reynolds number

Almério José V. P. S. Pamplona[a]

[a] *Universidade Federal de Goiás, Engenharia Mecânica, Goiânia, Goiás, Brazil*

Abstract

One uses the finite volume method with a staggered grid to numerically model the 2-D driven cavity flow in an unsteady state at Reynolds numbers equal 100, 400, 1000, 3200, 7500, and 10000. One validates the model by comparing it with well-established results in the literature.

Keywords: Finite Volume Method, Cavity, High-Reynolds

1. Introduction

The two-dimensional lid-driven cavity is a classical problem used to benchmark numerical methods in computational fluid dynamics. Thus, many authors have extensively studied this problem over the last forty years. Nallasamy and Prasad (1977) were one of the pioneers using a finite difference method based on an upwind difference scheme and the alternating direction line iterative method developed by the authors. Latter, Agarwal (1981) proposed a numerical model using a third-order-accurate upwind scheme for the convection terms and a central difference for the diffusion terms. In this scheme, both the convection and diffusion operators are third-order. A year after, Ghia et al. (1982) published a studying of the multigrid method combined with the finite difference method, using first-order accurate upwind and central difference schemes. Other authors produced several papers using the lid-driven cavity and applying other numerical methods. However, Ghia et al. (1982) stands out with his complete report, offering several table results.

Email address: almeriopamplona@gmail.com (Almério José V. P. S. Pamplona)

[1]

The present work aims to validate a code using the finite volume method. In this code the numerical model uses only the central difference scheme for convection and diffusion operators. Additionally, instead of a collocated uniform grid, one implements a staggered uniform grid to eliminate irrational oscillations. One introduces a description of the numerical model after the physical problem formulation. Then, one validates the code comparing the present and other authors' results.

2. Governing Equations

Consider a 2-D square cavity defined by the domain $\Omega = (0,1) \times (0,1)$ with $\Omega \subset \mathbb{R}^2$ and $T > 0$, $T \in \mathbb{R}$, as the simulation time. One describes an unsteady incompressible flow with a Newtonian fluid within the cavity by the continuity equation and the Navier-Stokes equations;

$$\begin{aligned}
&\frac{\partial \mathbf{u}}{\partial t} + (\mathbf{u} \cdot \nabla)\,\mathbf{u} = -\nabla p + \frac{1}{Re}\nabla^2 \mathbf{u}, && in\ [0,T] \times \Omega;\\
&\nabla \cdot \mathbf{u} = 0, && in\ [0,T] \times \Omega;\\
&\mathbf{u}\,(t,x,y) = (1,0), && on\ [0,T] \times \Gamma_1;\\
&\mathbf{u}\,(t,x,y) = (0,0), && on\ [0,T] \times \Gamma_0;\\
&\mathbf{u}\,(0,x,y) = (0,0), && in\,\Omega;
\end{aligned} \tag{1}$$

where $\mathbf{u} = (u, v)$ is the velocity field, p is the pressure field, Γ_1 is the top boundary, and Γ_0 represents the three other sides. Re is the Reynolds number, which is defined as $Re = U\,L/\nu$, where L is the characteristic length and U is larger velocity module in the flow field. For a square cavity, L is equal to the cavity's side, and U is equal to the lid's velocity.

3. Discretization with Finite Volume Method

One discretizes the flow domain into a uniform staggered grid G_h, fig. 1. A staggered grid has the advantage to prevent the decoupling of the pressure and velocity at adjacent grid points, which eliminates issues of irrational oscillations. The grid in the present work has a mesh size equal to the step discretization $(\Delta x, \Delta y)$, and the distance between the volumes' center has the same value $(\delta x = \Delta X, \delta y = \Delta y)$. The discrete values of the pressure are in the center of each finite volume. While discrete values of the velocity field are in the center of the staggering volumes.

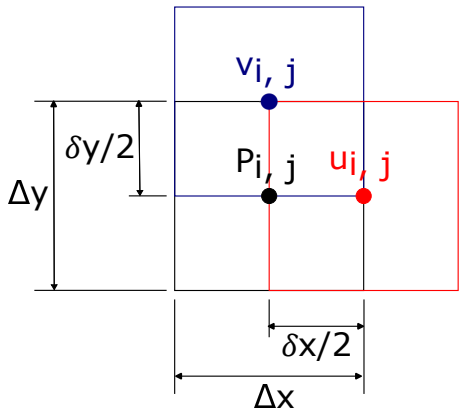

Figure 1: Staggering finite volumes (Ω_i) of the grid G_h.

Let the values on the finite volumes surfaces be the linear interpolation between discrete values in the center of the adjacent volumes and integrate the Navier-Stokes equations in eq. (1) on Ω_i and on $[t, t+\Delta t]$. This results in the following discrete form:

$$\begin{aligned}\hat{u}_{i,j}^{n+1} = \hat{u}_{i,j}^{n} &- \frac{1}{4}\frac{\Delta t}{\Delta x}\left[\left(\hat{u}_{i,j+1}^{n}+\hat{u}_{i,j}^{n}\right)^2-\left(\hat{u}_{i,j-1}^{n}+\hat{u}_{i,j}^{n}\right)^2\right]\\ &- \frac{1}{4}\frac{\Delta t}{\Delta y}\left[\left(\hat{u}_{i+1,j}^{n}+\hat{u}_{i,j}^{n}\right)\left(\hat{v}_{i,j+1}^{n}+\hat{v}_{i,j}^{n}\right)-\left(\hat{u}_{i-1,j}^{n}+\hat{u}_{i,j}^{n}\right)\left(\hat{v}_{i-1,j+1}^{n}+\hat{v}_{i-1,j}^{n}\right)\right]\\ &- \frac{\Delta t}{\Delta x}\left(p_{i,j+1}^{n}-p_{i,j}^{n}\right)+\frac{\Delta t}{Re\,\Delta x^2}\left(\hat{u}_{i,j+1}^{n}-2\hat{u}_{i,j}^{n}+\hat{u}_{i,j-1}^{n}\right)+\\ &\frac{\Delta t}{Re\,\Delta y^2}\left(\hat{u}_{i+1,j}^{n}-2\hat{u}_{i,j}^{n}+\hat{u}_{i-1,j}^{n}\right); \quad (2)\end{aligned}$$

$$\begin{aligned}\hat{v}_{i,j}^{n+1} = \hat{v}_{i,j}^{n} &- \frac{1}{4}\frac{\Delta t}{\Delta y}\left[\left(\hat{u}_{i+1,j}^{n}+\hat{v}_{i,j}^{n}\right)^2-\left(\hat{u}_{i-1,j}^{n}+\hat{v}_{i,j}^{n}\right)^2\right]\\ &- \frac{1}{4}\frac{\Delta t}{\Delta x}\left[\left(\hat{v}_{i,j+1}^{n}+\hat{v}_{i,j}^{n}\right)\left(\hat{u}_{i+1,j}^{n}+\hat{u}_{i,j}^{n}\right)-\left(\hat{v}_{i,j-1}^{n}+\hat{v}_{i,j}^{n}\right)\left(\hat{u}_{i+1,j-1}^{n}+\hat{u}_{i,j-1}^{n}\right)\right]\\ &- \frac{\Delta t}{\Delta y}\left(p_{i+1,j}^{n}-p_{i,j}^{n}\right)+\frac{\Delta t}{Re\,\Delta x^2}\left(\hat{v}_{i,j+1}^{n}-2\hat{v}_{i,j}^{n}+\hat{v}_{i,j-1}^{n}\right)+\\ &\frac{\Delta t}{Re\,\Delta y^2}\left(\hat{v}_{i+1,j}^{n}-2\hat{v}_{i,j}^{n}+\hat{v}_{i-1,j}^{n}\right). \quad (3)\end{aligned}$$

The hat symbol stands for the staggered velocity field, i and j represent the vertical and horizontal position indices, respectively, n describes the time, and Δt is the time step.

One must couple the velocity and pressure fields to preserve the mass and to keep the flow incompressibility property. One way to do that is through the Poisson equation, which requires a middle-step calculation due to the lack of information about the future velocities. The intermediate step gives a velocity approximation, which is the basis for the pressure approximation and the pressure correction. One can represent this procedure by the algorithm 1 where the tilde symbol stands for the approximated values, mometumEquationX and momentumEquationY represent the eqs. (2) and (3), respectively, and the bold variables represent the array form. The poissonEquation represents

Algorithm 1 Prediction-Correction algorithm

for $n \in [0, T]$ **do**
  for $i, j \in \Omega$ **do** ▷ Prediction step
    $\tilde{u}_{i,j} = \text{momentumEquationX}\left(\hat{u}^n_{i,j}, \hat{v}^n_{i,j}\right)$
    $\tilde{v}_{i,j} = \text{momentumEquaitonY}\left(\hat{u}^n_{i,j}, \hat{v}^n_{i,j}\right)$
  end for
  $\tilde{\mathbf{u}}, \tilde{\mathbf{v}} = \text{boundaryConditions}(\tilde{\mathbf{u}}, \tilde{\mathbf{v}})$
  $\tilde{p} = \text{poissonEquaton}(p^n, \tilde{\mathbf{u}}, \tilde{\mathbf{v}})$
  for $i, j \in \Omega$ **do** ▷ Correction step
    $p^{n+1}_{i,j} = p^n_{i,j} + \tilde{p}_{i,j}$
    $\hat{u}^{n+1}_{i,j} = \tilde{u}_{i,j} - \frac{\Delta t}{\Delta x}\left(\tilde{p}_{i,j+1} - \tilde{p}_{i,j}\right)$
    $\hat{v}^{n+1}_{i,j} = \tilde{v}_{i,j} - \frac{\Delta t}{\Delta y}\left(\tilde{p}_{i+1,j} - \tilde{p}_{i,j}\right)$
  end for
  $p^{n+1}, \hat{\mathbf{u}}^{n+1}, \hat{\mathbf{v}}^{n+1} = \text{boundaryConditions}\left(\hat{p^{n+1}}, \mathbf{u}^{n+1}, \hat{\mathbf{v}}^{n+1}\right)$
  if $\nabla \cdot \left(\hat{\mathbf{u}}^{n+1}, \hat{\mathbf{v}}^{n+1}\right) >$ tolerance **then**
    Stop: Mass is not conserved
  end if
end for

$$\tilde{p}_{i,j} = \breve{p}_{i,j} + \frac{\gamma}{2\Delta t}\frac{\Delta x^2\,\Delta y^2}{\Delta x^2+\Delta y^2}\left\{-2\Delta t\frac{\Delta x^2+\Delta y^2}{\Delta x^2\,\Delta y^2}\breve{p}_{i,j} + \frac{\Delta t}{\Delta x^2}\left(\breve{p}_{i,j+1}+\breve{p}_{i,j-1}\right) + \right.$$
$$\frac{\Delta t}{\Delta y^2}\left(\breve{p}_{i+1,j}+\breve{p}_{i-1,j}\right) - \frac{1}{\Delta x}\left(\tilde{u}_{i,j}-\tilde{u}_{i,j-1}\right) - \frac{1}{\Delta y}\left(\tilde{v}_{i,j}-\tilde{v}_{i-1,j}\right) +$$
$$\left. + \left[\frac{1}{\Delta x}\left(\tilde{u}_{i,j}-\tilde{u}_{i,j-1}\right) + \frac{1}{\Delta y}\left(\tilde{v}_{i,j}-\tilde{v}_{i-1,j}\right)\right]^2\right\}, \quad (4)$$

where γ is the under-relaxation coefficient and the brave symbol stands for the temporary values that the pressure assumes during successive iterations in the Gauss-Seidel method.

The boundary conditions on the west, east and bottom walls are ensured by the ghost volumes adjacent to the fluid volumes. Thus, the discrete values on those cells assume the values

$$v_{i,1} = -v_{i,2}; \quad v_{i,N} = -v_{i,N-1}; \quad u_{1,j} = -u_{2,j}, \quad (5)$$

where N is the total number of cells in one direction, counting the ghost ones. Meanwhile, the top wall or the lid moves with a constant value U_{lid}. Hence, the ghost cells must have the values

$$u_{N,j} = 2\,U_{lid} - u_{N-1,j}. \quad (6)$$

The final step in the algorithm 1 is a mass balance verification, which discrete form is

$$\nabla\cdot\mathbf{u} \approx \frac{1}{\Delta x}\left(u_{i,j}-u_{i,j-1}\right) + \frac{1}{\Delta y}\left(v_{i,j}-v_{i-1,j}\right). \quad (7)$$

4. Results

A representative solution of the flow structures with $Re = 100$, 400, 1000, 3200, 7500 and 10000 on a 128×128 grid, is shown in Figures 2. Each figure contains the velocity field and the streamlines. One represents the fields by the contour lines in the background, while the streamlines of the flow are the arrow lines on the plots. The time step used was 1×10^{-5} for $Re = 100$, 400, and 1000 with $t_{final} = 30\,s$, leading to an average processing time of 11198 s on a 128×128 grid and a laptop with an Intel(R) Core(TM) i5-8265U CPU,

1.60 GHz, 1.80 GHz and 12 GB RAM. For $Re = 3200$, $Re = 7500$, and 10000, the time step was 2×10^{-4} with $t_{final} = 660\,s$, resulting in $9576\,s$ of CPU time. Furthermore, One run a numerical experiment for $Re = 10000$ on a 256×256 grid with $\Delta t = 1 \times 10^{-5}$ and $t_{final} = 30\,s$. It took almost fourteen hours to complete, while the flow had not achieved a steady state.

Ghia et al. (1982) provides a result series of the lid cavity flow structures with $Re = 100$, 400, 1000, 3200, 7500, and 10000. In the present work, one does not make a direct comparison between Figure 2 and the ones in Ghia et al. (1982). However, it is worth mentioning that the results agreed very well. For instance, for $Re = 100$, both works have the central vortex near the lid and toward the left wall. Meanwhile, the vortices at the bottom right and left corners are relatively underdeveloped. For $Re = 400$, one observes in both papers that the center vortex moves toward the cavity's geometric center, and the corner vortices grow significantly. Finally, for $Re = 1000$, the center vortex stays at the same position that one observes in Figure 3. Nonetheless, it acquires lines with a more circular shape. The right corner vortex remains the same, while the left corner vortex develops more.

These results are also in agreement with Agarwal (1981). He pointed out that as $Re \to \infty$, the primary vortex becomes a centrally located, increasingly circular region of constant vorticity, essentially circumscribed by the boundaries of the cavity, which is the behavior observed through Figure 2. Agarwal (1981) also remarks that contrary to what people thought until 1981, for flows with high Reynolds number, the bottom corner vortices remain, and a third one appears at the top left corner. Ghia et al. (1982) went further and showed that up to $Re = 7500$, a secondary vortex appears in the bottom right corner and grows proportionally with the Reynolds number.

Figure 2: Streamlines and field contours showing solution on a 128×128 grid.

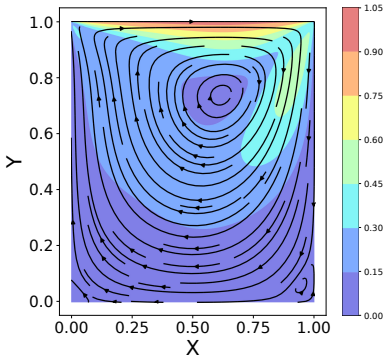

(a) $Re = 100$

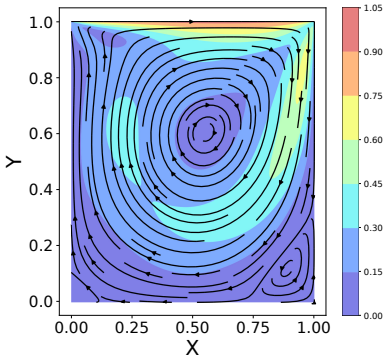

(b) $Re = 400$

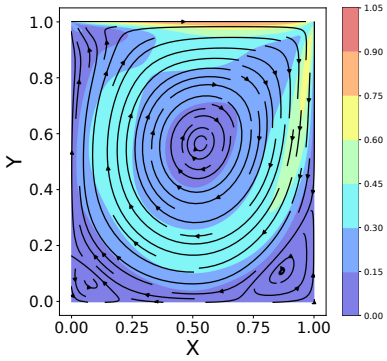

(c) $Re = 1000$

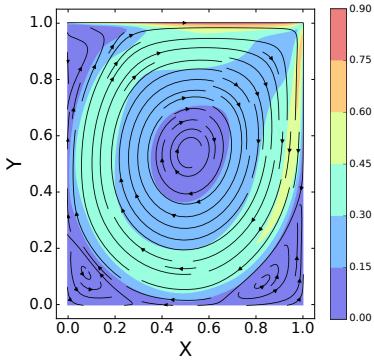

(d) $Re = 3200$

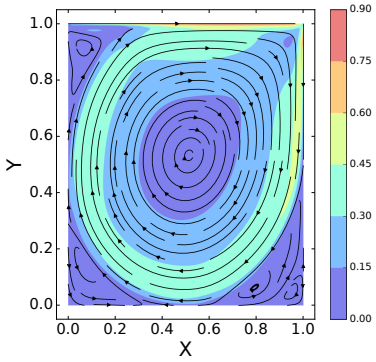

(e) $Re = 7500$

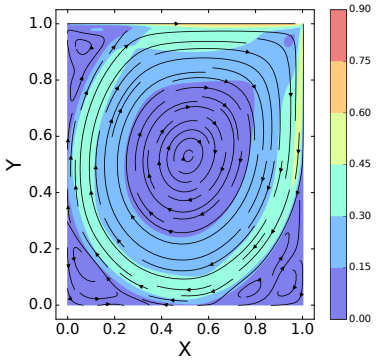

(f) $Re = 10000$

4.1. Velocity comparison

In order to validate the solution, one uses the velocity profiles in the cavity's midsection to compare with the literature results. One chosen the data from 129×129 and 257×257 grids in Ghia et al. (1982), a 121×121 grid in Agarwal (1981), and a 51×51 grid in Nallasamy and Prasad (1977). Figures 3, 4, 5, 6, 7, and 8 have the horizontal and vertical velocity profiles with Reynolds number equal to 100, 400, 1000, 3200, 7500, and 10000, respectively. The profiles have a good agreement with Ghia et al. (1982) results. However, Ghia et al. (1982) and the present work results have a significant difference relative to Agarwal (1981) and Nallasamy and Prasad (1977) profiles.

Figure 3: Comparison among the velocity profiles with Re = 100.

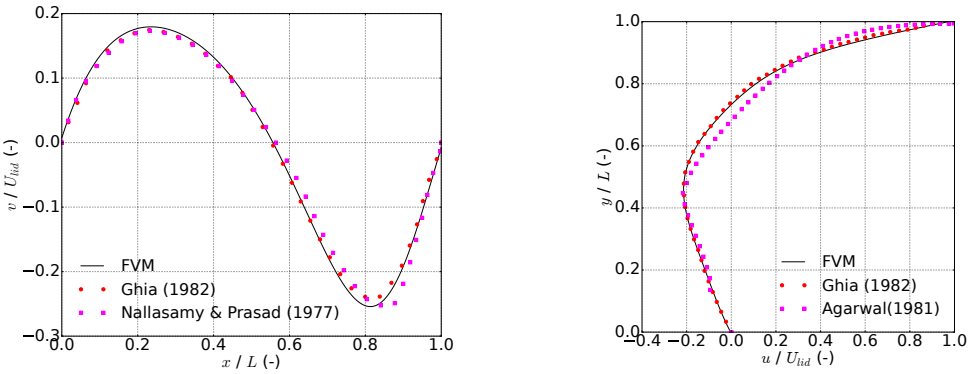

(a) vertical profile

(b) horizontal profile

In Figure 3b, one observes that for $y \in (0.4, 0.9)$, the fluid particles in Agarwal (1981) paper have greater horizontal velocity than in the Ghia et al. (1982) and the present work. However, for $Re = 400$, Figure 4b, the flow is faster in Agarwal (1981) for $y \in (0.0, 0.4)$, while it is slower for $y \in (0.7, 0.1)$. These distinctions may be explained by the different refinement among the grids, with Agarwal's grid being the coarser one.

In Figure 3a, one observes a good agreement among the three results. Nonetheless, the coarser grid in Nallasamy and Prasad (1977) significantly affects their results for $Re = 1000$ in Figure 5a. That shows that higher Reynolds numbers require finer grids to capture the flow structures accurately.

Figure 4: Comparison among the velocity profiles with Re = 400.

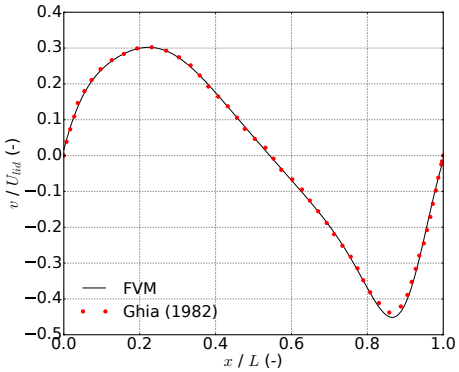

(a) vertical profile

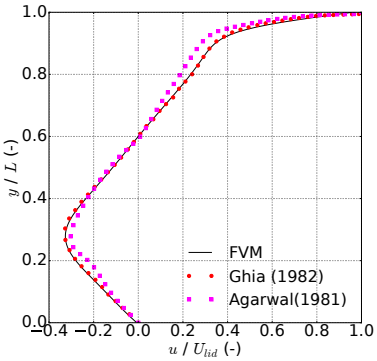

(b) horizontal profile

Figure 5: Comparison among the velocity profiles with Re = 1000.

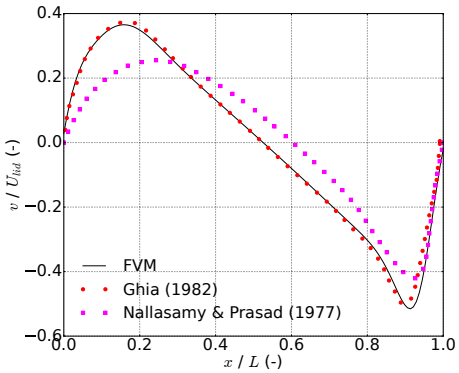

(a) vertical profile

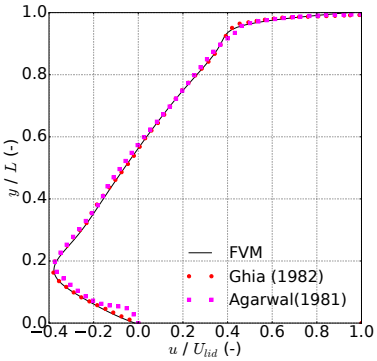

(b) horizontal profile

As the Reynolds number increases, one notes the dispersive effects of the central difference scheme (Morton and Mayers, 2005; LeVeque, 2007) used to model the convective term in Equation (1). There is no noticeable spurious oscillation in Figures 6, 7, and 8. However, one notes that the FVM's profile is slightly anitclockwise rotated relatively to Ghia et al. (1982) and Agarwal (1981). Thus, one could say that the distinct grid refinement is responsible for the deviation. Nonetheless, for $Re = 3200$, the literature result has virtually the same grid as the FVM, and one observes the difference between FVM

and the two authors, but not between Ghia et al. (1982) and Agarwal (1981). As a result, the grid is not the culprit.

Figure 6: Comparison among the velocity profiles with Re = 3200.

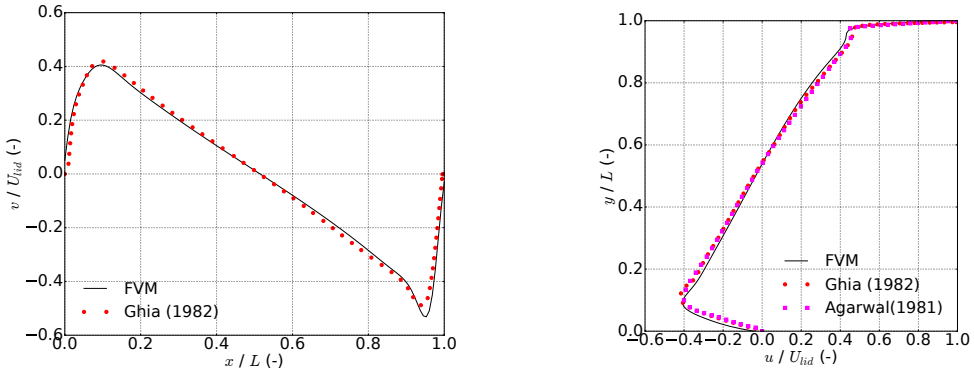

(a) vertical profile

(b) horizontal profile

Hence, the distinct numerical approaches may cause deviations. Ghia et al. (1982) and Agarwal (1981) used a mixed model, an upwind scheme for the convective term, and a central difference for the diffusive part. The upwind pattern has a significant dissipative effect, causing great artificial losses and diminishing accuracy. As a result, it damps the dispersive power of the central difference. Ghia et al. (1982) worked around the accuracy aspect, using the multigrid technique besides the finer grid, 257×257. Meanwhile, Agarwal (1981) used a third-order-accurate version of the upwind scheme.

The present work used the central difference pattern for diffusive and convective terms. Then, to resolve the oscillations, one used a staggered grid. The damping effect of the upwind and the staggered grid can be different, probably because they affect distinct oscillations frequency ranges. These may justify the deviation between the results. Furthermore, another probable influence is the numerical method to solve Poisson's equations. Agarwal (1981) used an alternating direction-line iterative algorithm, while Ghia et al. (1982) used a Gauss-Seidel relaxated process. In the current paper, one also used a Gauss-Seidel method, but without details from Ghia et al. (1982), one can guess that the parameters were different, leading to distinctive pressure field approximations.

Figure 7: Comparison among the velocity profiles with Re = 7500.

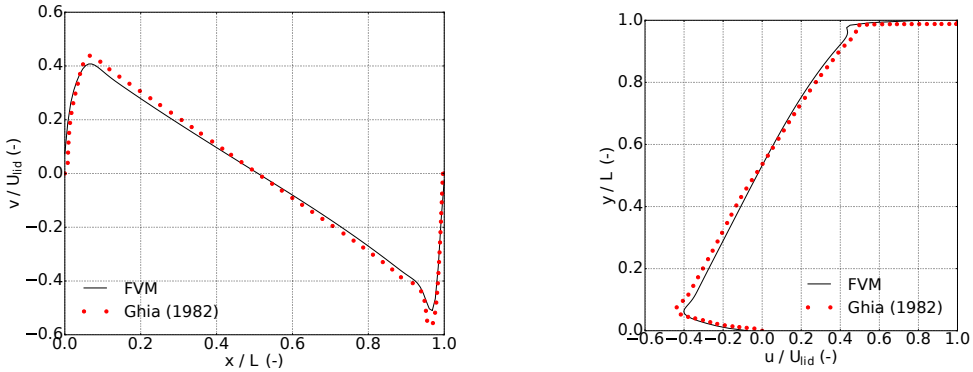

(a) vertical profile

(b) horizontal profile

Figure 8: Comparison among the velocity profiles with Re = 10000.

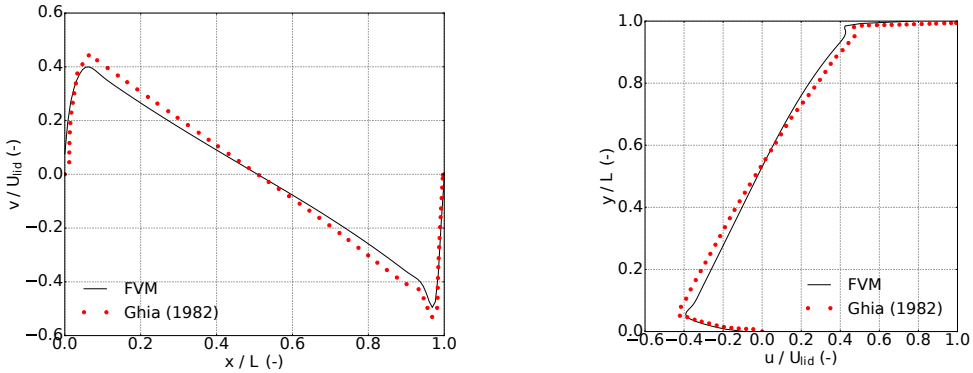

(a) vertical profile

(b) horizontal profile

5. Conclusions

Overall, the implemented numerical model has an exceptional agreement with the literature until $Re = 1000$. For Reynolds numbers greater than or equal to 3200, slight deviations become noticeable. One can consider the FVM results accurate because one justifies the differences by the distinct numerical techniques details, such as mixed (upwind and central differences) or pure schemes (only central differences with staggered grid), or different

methods to solve the Poisson's equation. Nevertheless, the code was properly validated.

One could implement further improvements to increase the time performance. The first one is a code translation from Python to C++. A second augmentation is a multigrid application, which is the technique that Ghia et al. (1982) used to speed his numerical solution. Finally, code parallelization would also reduce the processing time.

References

Agarwal, R.K., 1981. A third-order-accurate upwind scheme for navier-stokes solutions at high reynolds numbers. AIAA .

Ghia, U., Ghia, K.N., Shin, C.T., 1982. High-re solutions for incompressible flow using the navier-stokes equations and a multigrid method*. Journal of Computational Physics 48, 387–411.

LeVeque, R.J., 2007. Finite difference methods for ordinary and partial differential equations: Steady-state and time-dependent problems. Society for Industrial and Applied Mathematics, Philadelphia.

Morton, K.W., Mayers, D., 2005. Numerical solution of partial differential equations: An introduction. 2 ed., Cambridge University Press, Cambridge.

Nallasamy, M., Prasad, K.K., 1977. On cavity flow at high reynolds numbers. J. Fluid Mech 79, 391–414.